DETECTION OF OYSTER AND GROUNDWATER DISCHARGE IN TIDAL FLATS USING SYNTHETIC APERTURE RADAR

PI No.: 358

Duk-jin Kim[1], Byung-Hun Choe[1], Wooil M. Moon[2], Sang-Eun Park[3], Ji-Hwan Hwang[4], and Yisok Oh[4]

[1] School of Earth and Environmental Sciences, Seoul National University, Korea
[2] Geophysics, University of Manitoba, Canada
[3] Graduate School of Science and Technology, Niigata University, Japan
[4] Department of Electronics, Information and Communication Engineering, Hongik University, Korea

1. INTRODUCTION

Tidal flat, a transition zone between the ocean and land, forms a unique ecosystem, providing the habitat for various specious of fauna and flora, which is very important in purifying pollutants discharged from land and in providing marine products such as oysters and many kinds of shellfishes [1]. Thus, monitoring and mapping of tidal flat is urgently needed for sustainable managements and the conservation of tidal flats. However, tidal flat is very tough place to access and investigate. Microwave remote sensing technique can provide broad spatial coverage and temporally regular observations. Most studies using synthetic aperture radar (SAR) – one of the microwave remote sensing – have been conducted to extract surface geophysical parameters on bare soils or on vegetation areas. Very few studies have been carried out for monitoring and mapping of tidal flats [2-4].

Tidal flats can also be considered as bare soil, but they are different from typical bare soil from an electromagnetic scattering point of view. Furthermore, benthic fauna habitats in tidal flats can form a relatively rough surface by their unique structure or their survival activities. So they can make distinguished scattering signatures which are different from the background mud or sand flats.

In this study, we tried to extract the distribution of oyster reefs by analyzing their unique scattering characteristics from polarimetric SAR data. We also investigated why the oyster reefs can be generated naturally in these tidal flats.

2. STUDY AREA AND SAR DATA ACQUISITION

The study areas are Jebu Island and Hampyung Bay, the west coast of Korean peninsula (Fig. 1). The coast of Korean peninsula is famous for its large tidal range and wide tidal flats. It accounts for about 3% of the South Korea territory. SAR data were collected in multi-frequency and polarimetric mode over the study areas. TerraSAR-X, RADARSAT-2, and ALOS PALSAR are the space-borne polarimetric SAR systems that are currently available. We collected these three frequency and polarimetric SAR data over the study sites (Table 1). All SAR data were processed in Single Look Complex (SLC) for polarimetric analysis and then radiometrically and geometrically calibrated. Currently dual polarization TerraSAR-X data were used in this study.

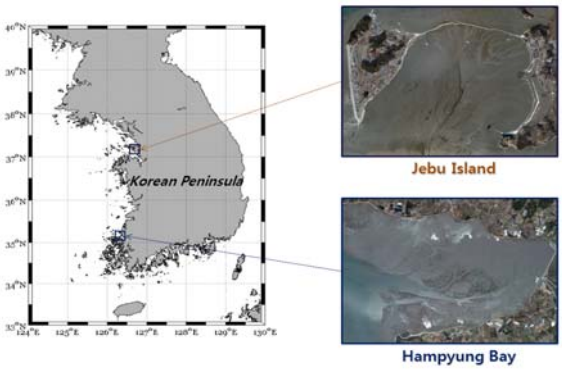

Fig. 1. Study areas. Right figures show the aerial photos of two study sites – Jebu Island and Hampyung Bay

	ALOS PALSAR	RADARSAT2	TerraSAR-X
Acquisition date	2007. 4. 13 / 2009. 4. 18	2008. 11. 20 / 2008. 12. 07	2008. 11. 20 / 2009. 01. 19
frequency	1.27 GHz (L-band)	5.405 GHz (C-band)	9.65GHz(X-band)
Polarization	HH/HV/VH/VV	HH/HV/VH/VV	VH/VV, HH/VV
Pixel resolution (range x azimuth)	9.3 x 3.5 m / 9.3 x 3.5 m	4.7 x 5.1 m / 4.7 x 5.5 m	0.9 x 2.4 m / 0.9 x 2.3 m
Incidence angle	22.7 ~ 24.9 ° / 22.6 ~ 24.9 °	35.4 ~ 37.0 ° / 30.2 ~ 31.9 °	22.4~24.2 ° / 39.0 ~ 40.3 °

	ALOS PALSAR	RADARSAT2
Acquisition date	2007. 12. 11	2010. 02. 26 / 2010. 03. 12
frequency	1.27 GHz (L-band)	5.405 GHz (C-band)
Polarization	HH/HV/VH/VV	HH/HV/VH/VV
Pixel resolution (range x azimuth)	9.3 x 3.5 m	4.7 x 4.8 m / 4.7 x 5.1 m
Incidence angle	7.4 ~ 13.0°	39.3 ~ 40.7 ° / 48.3 ~ 49.4 °

Table 1. SAR data acquisitions for Jebu Island (top) and Hampyung (bottom) study sites.

3. IN-SITU MEASUREMENTS

We obtained the C-band fully polarimetric data in tidal flats using a ground-based microwave scatterometer system. At the same time, we obtained surface roughness parameters (i.e., RMS height and correlation length) and soil moisture contents using the laser profiler system and soil sampling, respectively (Fig. 2)

Fig. 2. In-situ measurements using a ground-based scatterometer system and laser surface profiler.

The RMS height of oyster reefs was about 3 times greater than that of mud flats, and the correlation length of oyster reefs was about 2.5 times smaller than that of mud flats (Table 2).

	rms height (cm)	correlation length (cm)
Mud flats	0.66	9.44
Oyster reefs	1.87	3.67

Table 2. Average values of RMS height and correlation length. Eight surface profiles were averaged for the calculations.

We also established a transect line from land to seaward to compare the backscattering coefficient values from SAR data with the theoretical models (Integral Equation model and Oh's semi-empirical model). Surface roughness, soil moistures, and salinity were measured about 80m internals along the transact line (Fig. 3). Each location was surveyed using Total Station and Reflector. We also quantified the percentage of remnant water in depressions by classifying the each photo image into water and non-water area.

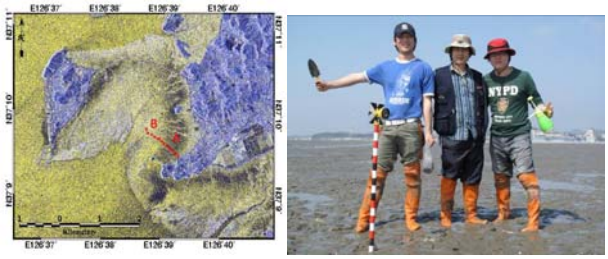

Fig. 3. Field measurements along a transact line in Jebu study area.

4. OYSTER DETECTION

4.1 Analysis methods

According to Freeman-Durden (FD) three component decomposition theorem, the covariance matrix of fully polarimetric SAR data can be decomposed to three scattering mechanisms [5] - the surface scattering, double-bounce scattering, and volume scattering;

$$[C_3]=\begin{bmatrix} f_s\beta^2 + f_d\alpha^2 + f_v & 0 & f_s\beta + f_d\alpha + \frac{f_v}{3} \\ 0 & \frac{2}{3}f_v & 0 \\ f_s\beta + f_d\alpha + \frac{f_v}{3} & 0 & f_s + f_d + f_v \end{bmatrix} \quad (1)$$

$$P = P_s + P_d + P_v = |S_{HH}|^2 + 2|S_{HV}|^2 + |S_{VV}|^2 \quad (2)$$

$$\text{with} \quad \begin{aligned} P_s &= f_s(1+\beta^2) \\ P_d &= f_d(1+\alpha^2) \\ P_v &= \frac{8}{3}f_v \end{aligned} \quad (3)$$

where f_s, f_d, f_v are the surface, double-bounce, and volume scattering contributions to the VV cross-polarized component. And α, β are the ratio of horizontal component to vertical component of the scattering matrix, in double-bounce scattering and surface scattering, respectively.

For quantitative comparison of the scattering mechanisms, each scattering proportion was normalized by [6].

$$N_{i\ (i=s,d,v)} = \frac{P_i}{P_s + P_d + P_v} \quad (4)$$

Depolarization means the polarization state of the transmitted signal changed by reacting to the target. In general, the strong depolarization can be occurred when multiple and volume scattering of target are dominant. The depolarization is usually calculated with three factors [7] - the cross-polarized ratio, co-polarized correlation, and co-polarized phase difference:

$$ratio_{cross-pol} = \frac{\left\langle |S_{HV}|^2 \right\rangle}{\left\langle |S_{VV}|^2 \right\rangle} \quad (5)$$

$$\rho_{HHVV} = \frac{\left\langle S_{HH} S_{VV}^{*} \right\rangle}{\sqrt{\left\langle |S_{HH}|^2 \right\rangle \left\langle |S_{VV}|^2 \right\rangle}} \quad (6)$$

$$\phi_{co-pol} = \phi_{HH} - \phi_{VV} = \arctan\left(\frac{\left\langle \mathrm{Im}(S_{HH}S_{VV}^{*})\right\rangle}{\left\langle \mathrm{Re}(S_{HH}S_{VV}^{*})\right\rangle}\right) \quad (7)$$

Higher value of cross-polarized ratio, smaller value of co-polarized correlation, and random distribution of co-polarized phase difference between 0° and ±180° usually represent a strong depolarization effect [8].

4.2 Oyster detection results

We applied Freeman-Durden three component decomposition to fully polarimetric C-band RADARSAT-2 data and L-band ALOS PALSAR data. Strong multiple and volume scattering were observed in the areas of oyster reefs in C-band RADARSAT-2 data, while only surface scattering was dominant in most tidal flat of L-band SAR data (Fig. 4). The normalized quantity of volume scattering in C-band SAR data had values greater than 0.8 in oyster reef areas. Strong depolarizations (greater than -4dB in the cross-polarized ratio, lower than 0.6 in the co-polarized correlation, and the co-polarized phase difference of between ±70° and ±180°) were also observed in oyster reef areas of C-band data (Fig. 5).
These unique scattering signatures were verified using the ground-based scatterometer measurements (Fig. 2). The ground-based scatterometer measurements also showed distinctive scattering characteristics between the oyster reefs and the mudflats. Radar backscatterings from the oyster reef were stronger in all polarizations (HH, HV, VH and VV) than from the mudflat. In particular, HV and VH cross-polarized backscatterings were significantly increased in oyster reef area. The significant increase in cross-polarization, relative to the co-polarization signals, can also be related to the depolarization effects. These scattering signatures were not observed in mud flat areas (Fig. 6). However, these depolarization effects were not observed in L-band SAR data. The sharp and jagged structure of oyster reef area may cause the transmitted C-band microwave signal depolarized, resulting in the increased radar backscattering in C-band HV and VH polarization. But such depolarization effects may not be occurred strongly in L-band microwave signal.
These results demonstrate that the microwave scattering behaviours can change according to the radar wavelength transmitted, and a proper wavelength of microwave can be selected to detect oyster signatures in tidal flats. We tested our findings to detect oyster reef area in tidal flats. When we applied the Freeman-Durden decomposition to SAR data of Hampyung Bay tidal flat, similar scattering characteristics were observed in this area. Strong volume scattering was observed in C-band SAR data, but such signatures were not observed in L-band SAR data (Fig. 7). In the areas of strong volume scattering in C-band SAR data, many oysters were found (Fig. 8).

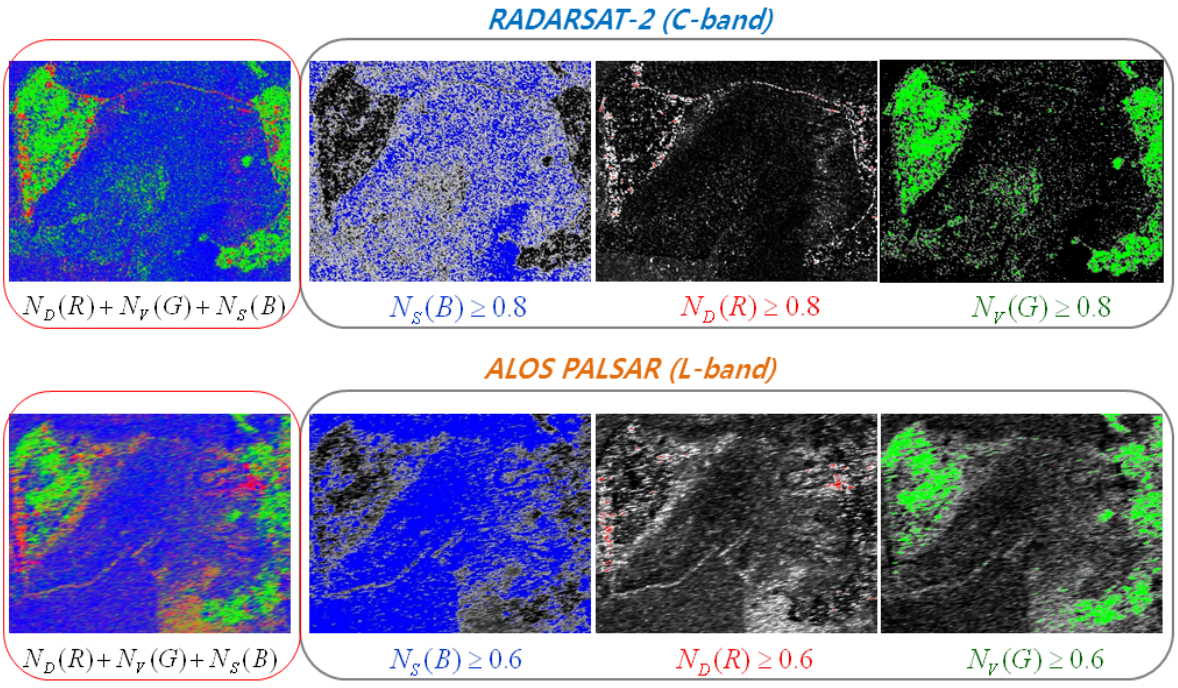

Fig. 4. Freeman-Durden three component decompositions of C-band RADARSAT-2 (top) and L-band ALOS PALSAR data (bottom). Three right figures show the each amount of surface (blue), double bounce (red), and volume scattering (blue), respectively.

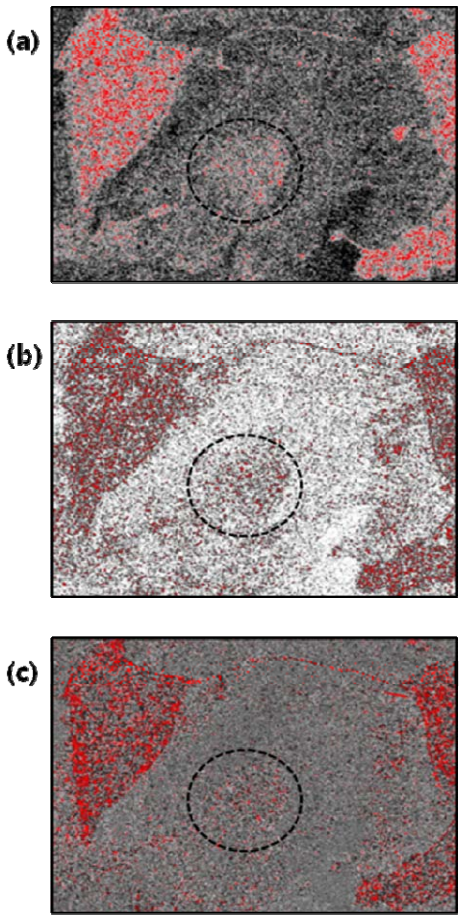

Fig. 5. The calculated depolarization effects from RADARSAT-2 (C-band) data. (a) Cross-polarized ratio (the values greater than -4dB are dotted in red), (b) Co-polarized correlation (the values below 0.6 are dotted in red), (c) Co-polarized phase difference (the values between -180° and -70° are dotted in red).

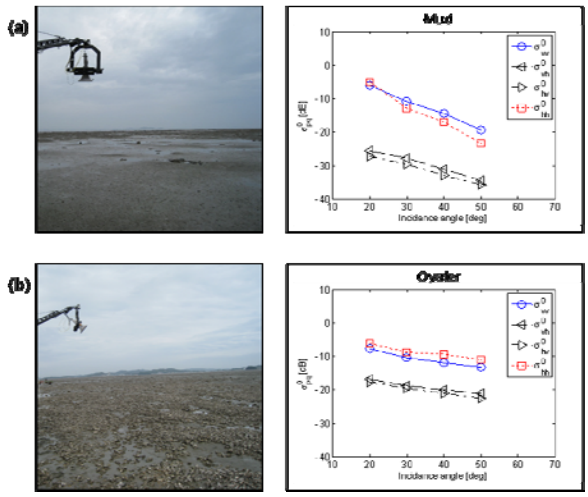

Fig. 6. Measurements of radar backscattering using a C-band ground-based microwave scatterometer system (left). (a) mud flat area (b) oyster reef area.

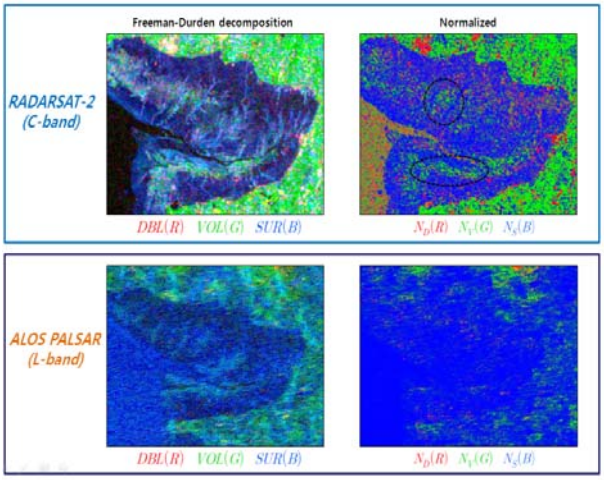

Fig. 7. The results of Freeman-Durden decomposition for Hampyung Tidal flat SAR data.

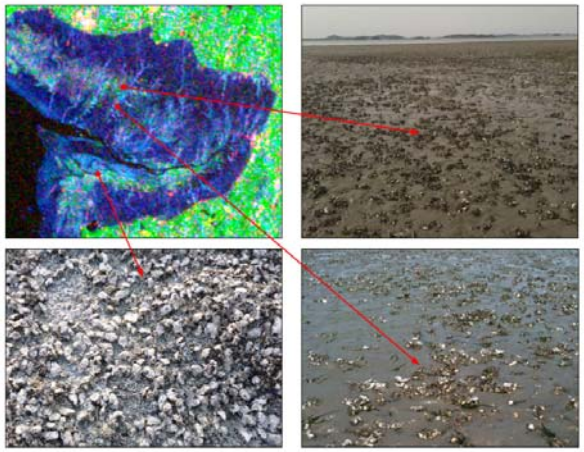

Fig. 8. Field verifications for the areas of strong volume scattering in Hampyung tidal flat.

5. GROUNDWATER DISCHARGE DETECTION

Because we were curious why the oysters were generated naturally in these tidal flats, further investigations were conducted. Many researches have reported that submarine groundwater discharge (SGD) plays an important role in transporting land nutrients to coastal ocean sea [9, 10]. We focused on this SGD to explain the distribution of oysters in tidal flats. Fig. 8 shows multi-frequency and multi-temporal SAR data over the Jebu tidal flat. In these SAR images, we can observe belt shaped and relatively darker area along the upper part of tidal flat, regardless of radar frequency and SAR data acquisition time (Fig. 9).
We calculated the backscattering coefficient values for X-, C-, and L-band SAR data using Integral Equation Model (IEM)[11] and Oh's semi-empirical model [12] by entering the surface parameters we obtained from field work along a transaction line shown in Fig. 3. We also

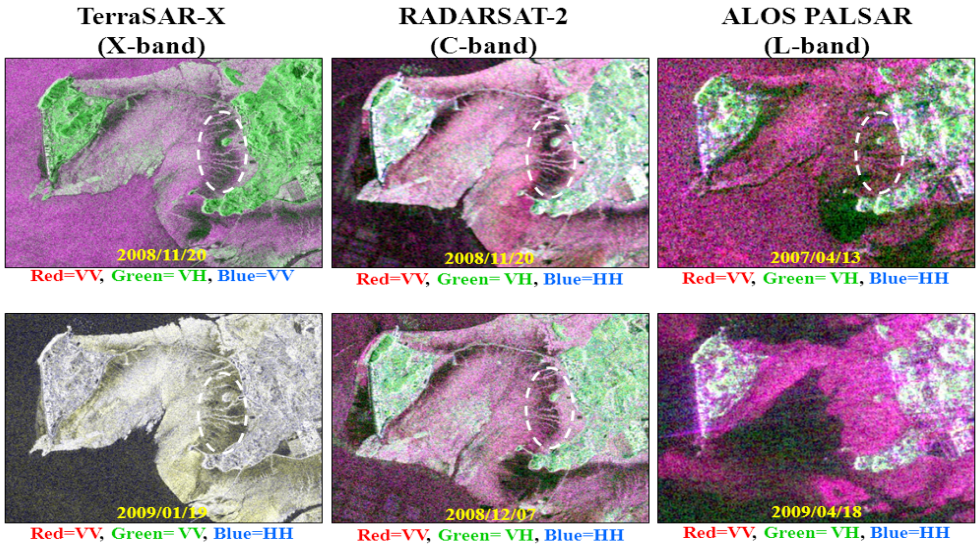

Fig. 9. Multi-frequency and multi-temporal SAR images over Jebu tidal flat. The white circles represent belt shaped and relatively dark area along the upper part of tidal flat.

derived the backscattering coefficient values from SAR data (Fig. 10).

The values of backscattering coefficient calculated from IEM and Oh model were not always agreed with the SAR data. Low SAR backscattering was observed in area *A*, while similar radar backscattering values were found in area *B*.

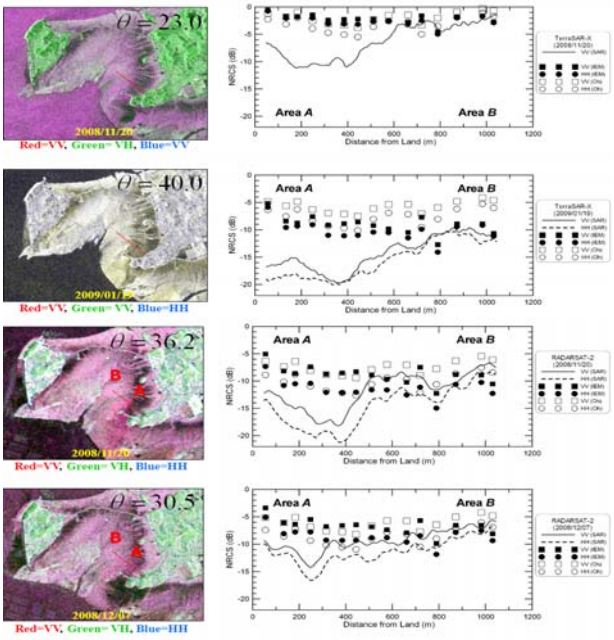

Fig. 10. Backscattering coefficient values along a transact line. The dark squares and circles represent the calculated values using IEM for VV and HH polarization, respectively. The white squares and circles are from Oh model. The solid and dashed lines were extracted from SAR data of VV and HH polarization, respectively.

We have investigated the tidal flat environment to find what caused the low SAR backscattering. As one can see in Fig. 11, the area A was partially covered with remnant water in puddles, while there was almost no water in area B. Because the surface roughness parameters were measured mostly for exposed sediments, excluding the actual water puddles, the backscattering coefficients calculated from the IEM and Oh models do not account for the contributions of these water puddles, which lowers the backscattering coefficient values due to specular reflection on the water surface.

Fig. 11. Photos of areas A and B.

However, we were still curious what made these environments in the tidal flat, because there were always water puddles in area *A*. The area *A* is closer to land than sea. If the water in the puddles is remnant water during ebb tide, the water puddles should be located closer to the sea, rather than closer to the land, because of their shorter exposure and evaporation time. However, this is clearly not the case. The numerous puddles forming belt shapes near the land are related to the geological setting of these areas, which eventually led us to conclude that these water puddles were generated from groundwater discharge. Actually, we found groundwater discharge in area *A* during the field work.

6. CONCLUSION AND DISCUSSIONS

We investigated the signature of oyster reefs in tidal flats from fully polarimetric SAR data and ground-based scatterometer data, using Freeman-Durden decomposition and depolarization factors. Laser profiler measurements showed a significant difference in surface roughness between oyster reefs areas and mud flats. Due to the rough structure of oyster reefs, strong cross-polarized (HV) backscattering and multiple scattering were observed in both C-band SAR data and ground-based scatterometer data. However, these scattering signatures were not observed in the L-band SAR data. Since the wavelength of L-band is about 4 times longer than that of C-band, the roughness difference between oyster reefs and mudflats was relatively small and negligible. Therefore, the distribution of oyster reefs in tidal flat can be extracted from C- and L-band polarimetric SAR data.

SGD plays an important role as a source of nutrients in many coastal waters. The study conducted here demonstrates that space-borne SAR systems are useful for identifying the spatial variations of surface roughness and the distribution of water puddles in tidal flats. If water puddles exist in a SAR resolution cell, darker areas will appear in the SAR image, indicating weakened radar backscattering due to specular reflection. Water puddles in a tidal flat can be variously formed depending on the topographical and geological features. If the darker areas of a SAR image (water puddles) are located closer to land in a tidal flat and they are belt shaped, they can be associated with groundwater discharge. Although our investigation does not cover all tidal flat areas worldwide, the approach and method presented in this paper will greatly assist in dramatically reducing laborious effort and time spent on searching for groundwater discharge with traditional measurement tools and approaches.

We can find these dark signatures in Jebu and Hampyung tidal flats. These tidal flats are famous for oyster reef area. Thus, we carefully conclude that the SGD seems to play an important role for the naturally generated oysters in the tidal flats.

REFERENCES

[1] H. Yokoyama and Y. Ishihi, Y., "Variation in food sources of the macrobenthos along a land-sea transect: a stable isotope study," *Mar Ecol Prog Ser.*, vol. 346, pp. 127-141, 2007.

[2] D. Van der wal, P.M.J. Herman, and A.W. Van den Dool, "Characterisation of surface roughness and sediment texture of intertidal flats using ERS SAR imagery," *Remote Sens. Environ.*, vol. 98, pp. 96-109, 2005.

[3] M. Gade, W. Alpers, C. Melsheimer, and G. Tanck, "Classification of sediments on exposed tidal flats in the German Bight using multi-frequency radar data," *Remote Sens. Environ.*, vol. 112, pp. 1603-1613, 2008.

[4] S.E. Park, W.M. Moon, and D.J. Kim, "Estimation of surface roughness parameter in intertidal mud flat using airborne polarimetric SAR data," *IEEE Trans. Geosci. Remote Sens.*, vol. 47(4), pp. 1022-1031, 2009.

[5] A. Freeman, and S.L. Durden, "A three-component scattering model for polarimetric SAR data," *IEEE Trans. Geosci. Remote Sens.*, vol. 36(3), pp. 969-973, 1998.

[6] S.K. Lee, S.H. Hong, S.W. Kim, Y. Yamaguchi, and J.S. Won, "Polarimetric features of oyster farm observed by AIRSAR and JERS-1," *IEEE Trans. Geosci. Remote Sens.*, vol. 44(10), pp. 2728-2735, 2006.

[7] J. Jensen, *Remote sensing of the environment*, Pearson Prentice Hall, NJ, pp.313-327, 2007.

[8] F.T. Ulaby, D. Held, M.C. Dobson, K.C. Mcdonald, and T.B.A. Senior, "Relating polarization phase difference of SAR signals to scene properties," *IEEE Trans. Geosci. Remote Sens.*, vol. GE-25(1), pp. 83-92, 1987.

[9] W. Burnett, H. Bokuniewicz, M. Huettel, W. Moore, and M. Taniguchi, "Groundwater and pore water inputs to the coastal zone," *Biogeochemistry*, vol. 66, pp. 3-33, 2003.

[10] W.S. Moore, "The role of submarine groundwater discharge in coastal biogeochemistry," *Journal of Geochemical Exploration*, vol. 88, pp. 389-393, 2006.

[11] A. Fung, Z. Li, and K. Chen, "Backscattering from a randomly rough dielectric surface," *IEEE Trans. Geosci. Remote Sens.*, vol. 30, pp. 356-369, 1992

[12] Y. Oh, K. Sarabandi, and F. Ulaby, "Semi-empirical model of the ensemble-averaged differential Mueller matrix for microwave backscattering from bare soil surface," *IEEE Trans. Geosci. Remote Sens.*, vol. 40, pp. 1348-1355, 2002.